

LAPTH-887/01
LPT-Orsay 01-105
IPPP/01/68
DCPT/01/136
December 2001

A NLO calculation of the large- p_T photon + photon \rightarrow photon + jet cross section

M. Fontannaz^(a), J. Ph. Guillet^(b), G. Heinrich^(c)

^(a) *Laboratoire de Physique Théorique, UMR 8627 CNRS,
Université Paris XI, Bâtiment 210, 91405 Orsay Cedex, France*

^(b) *LAPTH, UMR 5108 du CNRS associée à l'Université de Savoie,
BP 110, Chemin de Bellevue, 74941 Annecy-le-Vieux Cedex, France*

^(c) *Department of Physics, University of Durham, Durham DH1 3LE, England*

Abstract

We study the production of an isolated large- p_T photon as well as the production of an isolated prompt photon plus a jet in e^+e^- collisions. Our results are obtained by a NLO Monte Carlo program of partonic event generator type. We discuss the possibilities to constrain the parton densities in the real photon and compare to preliminary OPAL data.

1 Introduction

Hard reactions involving real photons, such as the photoproduction of jets [1, 2, 3, 4, 5] or of large- p_T photons [6, 7, 8, 9, 10], are often presented as good tests of QCD. Indeed the real photon having a pointlike coupling to a quark of the hard subprocess is a good probe of the short distance dynamics. This would particularly be the case if one could forget the hadronic component of real photons. In the initial state, the incoming real photon can fluctuate into states made of quarks and gluons which take part in the hard scattering process. This mechanism, referred to as the resolved process, leads to the introduction of quark and gluon distributions in real photons. Similarly a final state large- p_T photon can also be produced by the fragmentation of a large- p_T parton emerging from the hard scattering process ; this process is described by introducing the fragmentation function of partons into real photons. Therefore the reactions involving real photons are far from being simple processes and contain the whole complexity of the pure hadronic collisions. This is particularly true for the reaction $\gamma\gamma \rightarrow \gamma + X$ in which the final photon is produced at large transverse momentum. Each of the photons can have a direct or a resolved interaction such that eight different processes contribute to the cross section.

However this complexity has a positive aspect if the various contributions to the cross section can be disentangled by means, for instance, of kinematical cuts. In an ideal situation it should be possible to separately observe direct contributions which provide unambiguous tests of QCD, resolved contributions leading to the measurement of the quark and gluon distributions in the photon and fragmentation contributions giving access to the quark and gluon fragmentation functions. These fragmentation contributions can be strongly suppressed by using isolation criteria [11, 12] which eliminate events with a too large hadronic transverse energy in a cone surrounding the photon. For instance the criterion used by the OPAL experiment [13], that we analyze in this paper, completely suppresses the fragmentation contri-

bution and the remaining contributions to the cross section are due to direct and resolved incoming photons, the final photon being always a direct one.

One way to disentangle the resolved contribution from the direct one rests on the measurement of the momentum of the parton entering the hard subprocess [1] (a measurement which requires the observation of the whole final state). When the ratio of this momentum to the incoming photon momentum is close to one, one expects the direct contribution to be dominant (the photon momentum is not shared among the quarks and gluons) ; for a ratio smaller than one the resolved contribution is the larger one. One interesting aspect of the $\gamma + \gamma \rightarrow \gamma + X$ reaction at LEP II energies is that the dominant contributions to the cross section contain at least one resolved photon in the initial state. The direct-direct correction is negligible, and the observation of the $\gamma + \gamma \rightarrow \gamma + X$ cross section opens the possibility to measure the parton distributions in the photon.

Another interesting point of the reaction $\gamma + \gamma \rightarrow \gamma + X$ at LEP II energies is the small contribution of the NLO corrections. As we shall see below, these corrections represent – for the scales set equal to $p_{T\gamma}$ – about 10 % of the cross section. This result shows that the QCD corrections are well under control. Moreover the scale dependence is very weak and therefore the theoretical predictions are unambiguous.

The possibility to constrain the parton distributions in the photon, especially the rather poorly known gluon distribution, via the process $\gamma + \gamma \rightarrow \gamma + X$ has already been pointed out in [14, 15]. While [14] is a leading order calculation, in [15] the calculation is done at next-to-leading order, but only the fully inclusive cross section is calculated, without the possibility to consider isolated photons or a photon + jet final state.

The plan of the paper is the following. Section 2 is devoted to the theoretical framework and to the discussion of predictions for the inclusive cross sections $d\sigma/dp_{T\gamma}$ and $d\sigma/d\eta_\gamma$. In Section 3 we study the reaction $\gamma + \gamma \rightarrow \gamma + jet + X$, emphasizing the difference to the inclusive case. Comparisons with preliminary re-

sults of the OPAL experiment are performed in Section 4. Section 5 contains the conclusion.

2 Theoretical Framework and Predictions

2.1 General Setting

As the general framework of the calculation has already been described in detail in [16, 9, 5], we will give only a brief overview on the method here.

In e^+e^- reactions, the electrons can act like a source of quasi-real photons whose spectrum can be described by the Weizsäcker-Williams formula

$$f_\gamma^e(y) = \frac{\alpha_{em}}{2\pi} \left\{ \frac{1 + (1 - y)^2}{y} \ln \frac{Q_{max}^2(1 - y)}{m_e^2 y^2} - \frac{2(1 - y)}{y} \right\} . \quad (1)$$

This approximation is valid as long as $Q_{max}^2/p_T^2 \ll 1$ where p_T is a large scale characterizing the hard subprocess, for instance the transverse momentum of the final photon. In this section we use this approximation, postponing to Section 4 a discussion of its validity when comparing our predictions with OPAL data.

The quasi-real photon then either takes part *directly* in the hard scattering process, or it acts as a composite object, being a source of partons which take part in the hard subprocess. The latter mechanism is referred to as *resolved* process and is parametrized by the photon structure functions $F_{a/\gamma}(x_\gamma, Q^2)$. Thus the distribution of partons in the electron is given by the convolution

$$F_{a/e}(x_e, M) = \int_0^1 dy dx_\gamma f_\gamma^e(y) F_{a/\gamma}(x_\gamma, M) \delta(x_\gamma y - x_e) \quad (2)$$

where in the “direct” case $F_{a/\gamma}(x_\gamma, M) = \delta_{a\gamma} \delta(1 - x_\gamma)$.

Similarly, a high- p_T photon in the final state can either originate directly from the hard scattering process or it can be produced by the fragmentation of a hard parton emerging from the hard scattering process. However, as discussed in the introduction, this fragmentation contribution can strongly be suppressed by using

an isolation criterion. It turns out that this isolation is also useful at the experimental level in order to single out the prompt photon events from the background of secondary photons produced by the decays of light mesons. The isolation criterion used by the OPAL collaboration is the one proposed by Frixione [11] which leads to a complete suppression of the fragmentation contributions (contributions involving the fragmentation function $D_a^\gamma(z, M^2)$ of parton a into a photon). At the parton level we have the following constraints : for each parton i , the distance

$$R_{i\gamma} = \sqrt{(\phi_i - \phi_\gamma)^2 + (\eta_i - \eta_\gamma)^2} \quad (3)$$

to the photon is computed in (ϕ, η) space, where ϕ and η are the azimuthal angle and pseudorapidity, respectively. A photon is kept if the condition

$$\sum_i E_{T,i} \Theta(\delta - R_{i\gamma}) \leq 0.2 \cdot E_{T,\gamma} \frac{1 - \cos(\delta)}{1 - \cos(R)} \quad , \quad \text{for all } \delta \leq R \quad (4)$$

is fulfilled, where $E_{T,i}$ is the transverse energy of the i^{th} parton, Θ is the step function, which ensures that only particles in the cone with aperture δ contribute to the sum, and the cone radius is $R = 1$.

As a result, we only have to consider contributions with a direct final photon. These can be classified by the three production mechanisms illustrated in Fig. 1 : 1) direct-direct, 2) single resolved, 3) double resolved. Note that by "single resolved" we denote the sum of direct-resolved and resolved-direct contributions.

We implemented the full set of next-to-leading order corrections to the single resolved and double resolved processes. Note that the direct-direct process is by itself a higher order correction ; there is no Born contribution involving a $2 \rightarrow 2$ subprocess in this reaction. The isolation criterion does not modify the leading order contributions for the direct-resolved and resolved-resolved case shown in Fig. 1. But at NLO a parton can be close to the photon in the (ϕ, η) plane and the cross section is modified by the constraint (4).

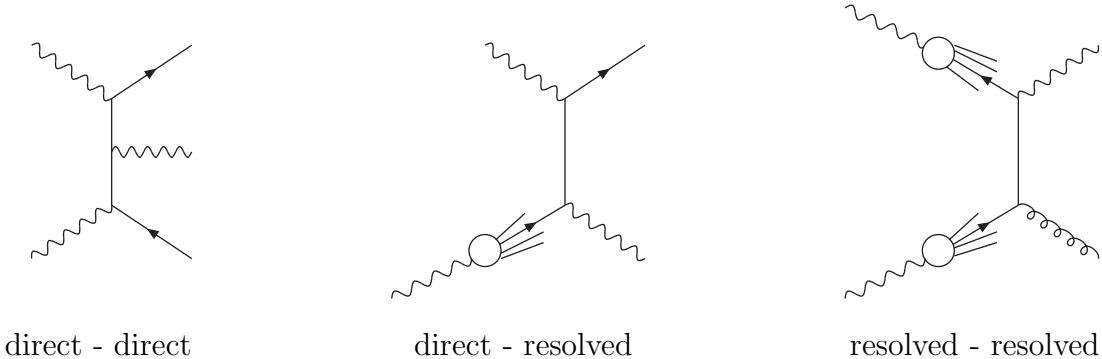


Figure 1: Examples of contributing processes.

In the calculation of the higher order corrections a phase-space slicing method is used which allows to isolate and analytically calculate the divergent infrared and collinear contributions. The non-divergent parts of the $2 \rightarrow 3$ contributions are calculated numerically. A partonic event generator (allowing negative weights) has been built on these bases. The interested reader may find a detailed description of this generator in ref. [16].

2.2 Predictions

Let us now study the NLO cross section of the $e^+e^- \rightarrow e^+e^-\gamma X$ reaction obtained in the above theoretical framework and by using the OPAL kinematical conditions. Thus we use $\sqrt{S_{e^+e^-}} = 196.6$ GeV, $Q_{max}^2 = 10$ GeV 2 and $0 \leq y \leq 1$. We also use the AFG parton distributions [17] and the value $\Lambda_{MS}^{(4)} = 300$ MeV. (We work with 4 flavours). The factorization scale M and the renormalization scale μ are set equal to $p_{T,\gamma}$. The NLO cross sections $d\sigma/dp_{T,\gamma}$ associated with the different production mechanisms, integrated in the rapidity range $-1 \leq \eta_\gamma \leq 1$, are displayed in Fig. 2.

For the scales $\mu = M = p_{T,\gamma}$ used here the single resolved contribution is larger than the double resolved contribution by a factor 3 to 6 which increases when $p_{T,\gamma}$ increases. The single resolved contribution constitutes about 70 % of the total cross

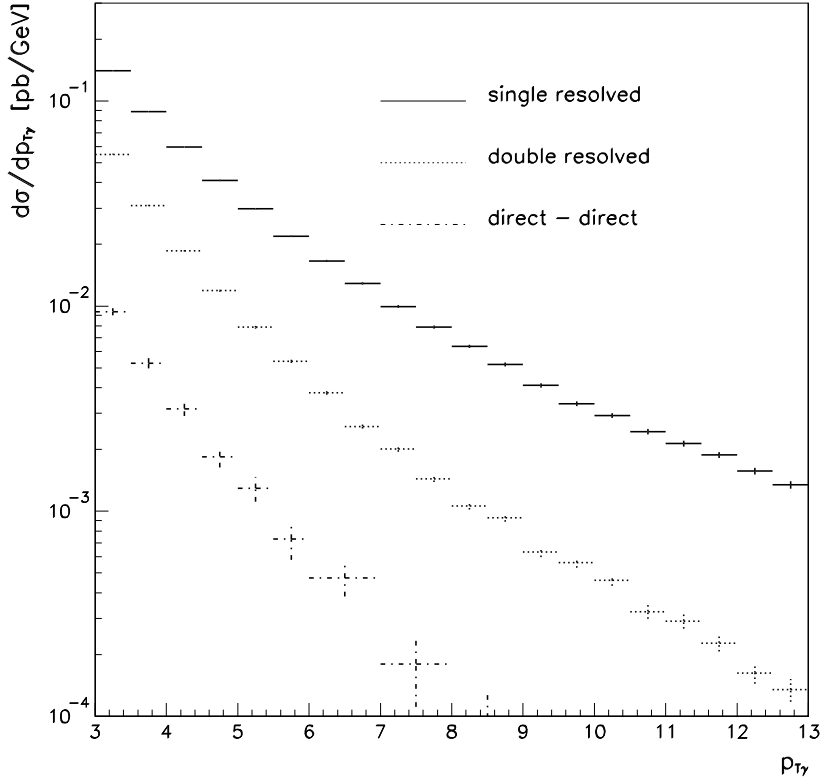


Figure 2: The NLO single resolved, double resolved and direct cross sections $d\sigma^{\gamma+X}/dp_{T\gamma}$.

section.

The ratio of the HO corrections to the NLO ($= \text{LO} + \text{HO}$) cross sections is displayed in Fig. 3. The HO corrections are small for the single resolved cross section ($\text{HO}/(\text{LO} + \text{HO}) \simeq 0.1$) and large for the resolved-resolved case ($\text{HO}/(\text{LO} + \text{HO}) \simeq 0.5$). The direct-direct HO contribution is smaller than the single resolved HO contribution ; it becomes negative at large $p_{T\gamma}$ ($p_{T\gamma} \gtrsim 10$ GeV). On this occasion we remind the reader that the individual contributions to the cross section are not physical. They depend on the factorization and renormalization scheme (here the \overline{MS} scheme). For instance the direct-direct HO contribution comes from the

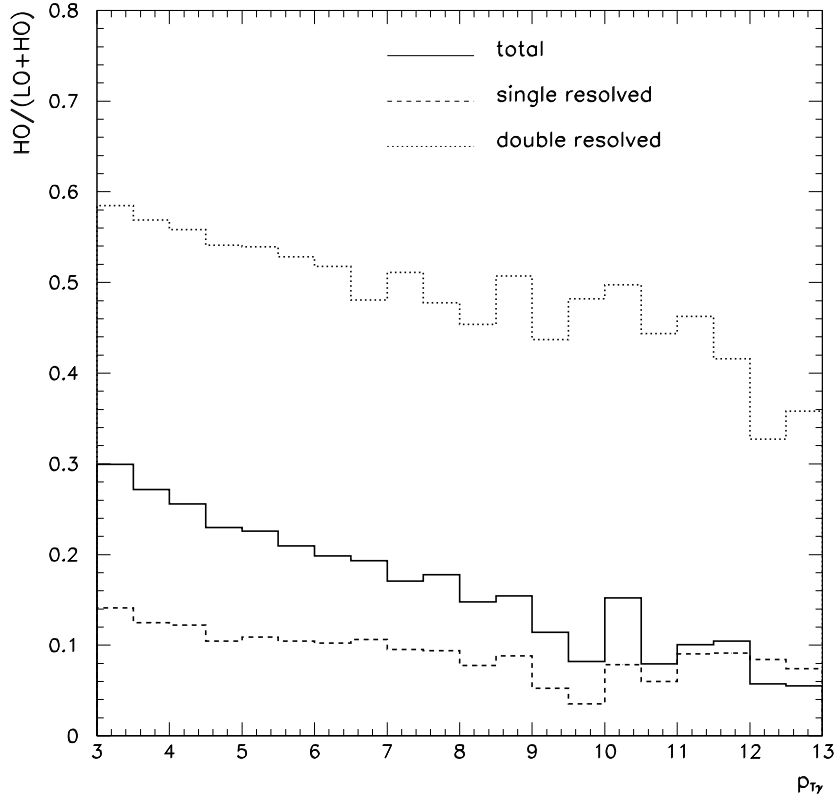


Figure 3: Ratios $\text{HO}/(\text{LO} + \text{HO})$ for the $e^+e^- \rightarrow e^+e^-\gamma X$ cross section, calculated with the scale $\mu = M = p_{T\gamma}$, as a function of $p_{T\gamma}$.

$\gamma + \gamma \rightarrow \gamma + q + \bar{q}$ cross section from which the initial state collinear divergences have been subtracted in the \overline{MS} -scheme. The finite remainders of the subtracted singularities depend strongly on the factorization scale M , this dependence being compensated only when adding the single resolved contributions.

Let us turn to the question of the stability of the predictions with respect to the choice of the renormalization and factorization scales. In Fig. 4 we display the variation of the cross section $d\sigma/dp_{T\gamma}$ calculated at $p_{T\gamma} = 6$ GeV as a function of the parameter C which defines the scale choice, $\mu = M = C p_{T\gamma}$ resp. $M = C p_{T\gamma}$; the cross sections are normalized to one at $C = 1$. The increase of the leading

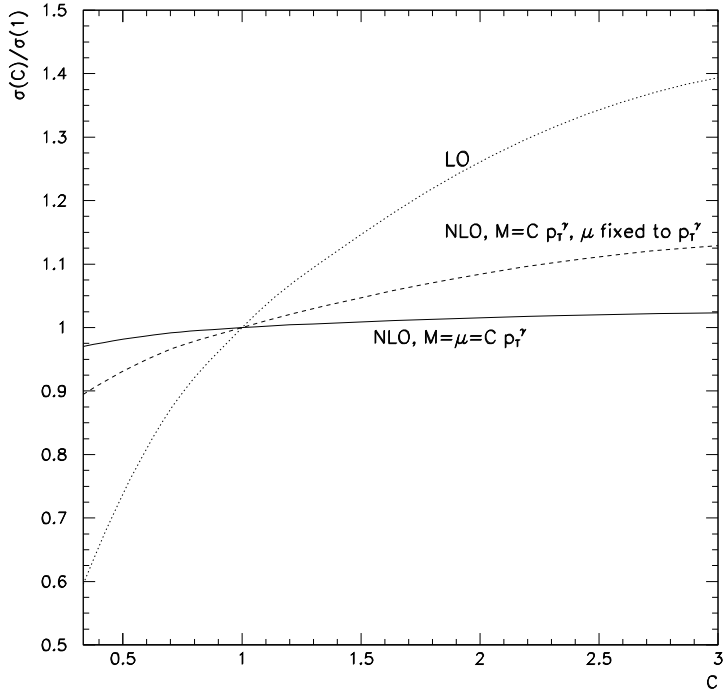


Figure 4: The dependence of $d\sigma^{\gamma+X}/dp_{T\gamma}$ at $p_{T\gamma} = 6$ GeV on the renormalization and factorization scales as a function of C . Solid line: $\mu = M = C p_{T\gamma}$ (NLO), dotted line: $\mu = M = C p_{T\gamma}$ (LO), dashed line: μ fixed to $p_{T\gamma}$, M varied between $p_{T\gamma}/3$ and $3 p_{T\gamma}$ (NLO).

order* cross section with increasing scales reflects the fact that – in contrast to the hadronic structure functions which show the well known scaling violations – the photon structure functions grow uniformly like $\log(Q^2/\Lambda^2)$ for large Q^2 since the pointlike piece dominates at large Q^2 .

We note that the variations of the NLO cross section are smaller than 5 %, when the values of the scales M and μ are changed simultaneously by a factor 9. At the same time, each individual cross section strongly varies. For instance the direct-

*What we denote by "leading order" only refers to the matrix elements. For the parton distributions we always use the NLL fits, and for α_s we use an exact solution of the two-loop renormalization group equation, and not an expansion in $\log \mu/\Lambda$.

direct contribution varies from 7.85×10^{-3} pb to -6.67×10^{-3} pb whereas the total cross section is equal to 23.82×10^{-3} pb at $C = 1$. If we vary the factorization scale M only, keeping μ fixed to p_{T_γ} , the variations of the NLO cross section are of course larger since cancellations of $\log p_{T_\gamma}^2/M^2$ and $\log \mu^2/p_{T_\gamma}^2$ terms are spoiled, but they are still only of the order of 20% for a variation of M^2 by almost two orders of magnitude, as can be seen from Fig. 3.

To conclude this short study of the cross section $d\sigma/dp_{T_\gamma}$ we can say that the NLO calculation is well under control ; the HO corrections are small and the sensitivity of the cross section to the scales is negligible. Therefore the reaction $e^+e^- \rightarrow e^+e^-\gamma X$ offers interesting tests of QCD and should allow to put constraints on the parton distributions in the real photon.

The cross section $d\sigma/d\eta_\gamma$ is a good observable to determine $F_{a/\gamma}(x, M)$, because the value of x is closely related to the value of η_γ . As a consequence the shape of $d\sigma/d\eta_\gamma$ gives indications on the x -dependence of the parton distributions in the photon. The cross sections $d\sigma/d\eta_\gamma$ are shown in Fig. 5 for $p_{T_\gamma} \geq 3$ GeV. Obviously the result is symmetric with respect to $\eta_\gamma = 0$ within the statistical errors. The box contribution $\gamma g \rightarrow \gamma g$ to the single resolved part is of the order of 5% of the total single resolved contribution, and of the same order of magnitude as the direct-direct contribution. However, in view of other uncertainties of the order of 5% (see Section 4), it has not been included in the results shown. The box correction $gg \rightarrow \gamma g$ to the double resolved part is one order of magnitude smaller than the $\gamma g \rightarrow \gamma g$ box and therefore completely negligible.

Large values of η_γ enhance the direct-resolved contribution (where the incoming direct photon goes towards positive rapidity). The resolved-resolved contribution is quite flat and the direct-direct one almost negligible (at the scales $\mu = M = p_{T_\gamma}$). A value of $p_{T_\gamma}^{min}$ larger than 3 GeV would enhance the single resolved cross section with respect to the double resolved one.

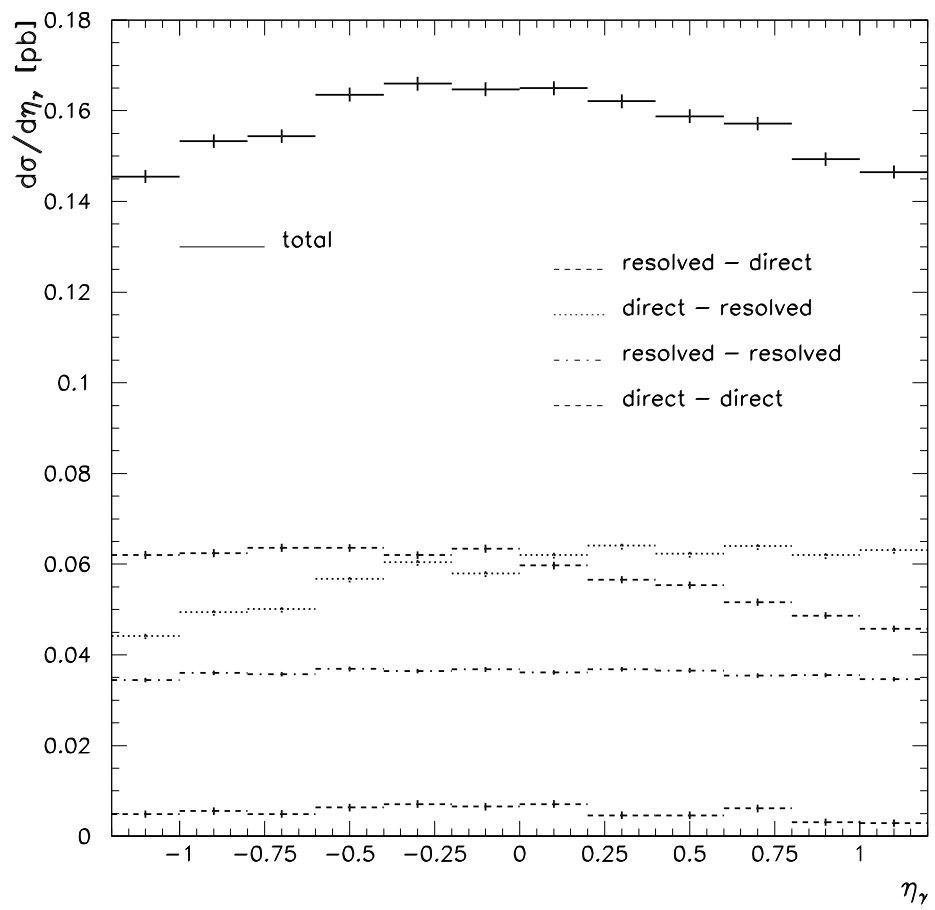


Figure 5: The cross section $d\sigma^{\gamma+X}/d\eta_\gamma$ as a function of η_γ for $p_{T\gamma} \geq 3$ GeV.

3 Photon-jet cross section

In the introduction, we discussed the possibility to enhance a resolved contribution with respect to a direct one by fixing the momentum of the partons entering the hard subprocess. Following the OPAL collaboration, we define

$$x^\pm = \frac{(E_{jet} \pm p_z^{jet}) + (E_\gamma \pm p_z^\gamma)}{\sum_{had,\gamma} (E \pm p_z)} = \frac{p_T^{jet} e^{\pm \eta_{jet}} + p_T^\gamma e^{\pm \eta_\gamma}}{y^\pm \sqrt{S_{e^+e^-}}} \quad (5)$$

where y^\pm are the fractional momenta of the quasi-real initial photons oriented towards the positive and negative z -axis, $y = E_\gamma/E_e$. The conventions are such that particle one travels towards the positive z -direction, such that e.g. direct-resolved means that the direct photon – with momentum fraction x_γ^+ – moves to positive z whereas the resolved photon (with momentum fraction x_γ^-) moves to negative z . The variables x^\pm defined by eq. (5) are exactly the longitudinal momentum fractions (with respect to the photon momenta) of the partons entering the hard subprocess if the latter is a $2 \rightarrow 2$ process. In the case of a $2 \rightarrow 3$ subprocess, these momentum fractions are no more fixed by the observation of the photon and a jet since there are configurations with a third (unobserved) particle in the final state such that the true value of x_γ^\pm in $F_{a/\gamma}(x_\gamma^\pm, M)$ (see eq. (2)) can be larger than x^\pm . Nevertheless x^\pm remain useful variables to constrain the parton momenta.

The definition (5) implies to measure the jet rapidity and transverse energy. In ref. [5] we defined another variable which does not require the measurement of p_T^{jet} ,

$$x_{LL}^\pm = \frac{p_T^\gamma (e^{\pm \eta_{jet}} + e^{\pm \eta_\gamma})}{y^\pm \sqrt{S_{e^-e^+}}} \quad . \quad (6)$$

This is certainly an advantage with respect to expression (5), because the measurement of a jet transverse energy at small p_T^{jet} ($p_T^{jet} \sim 5$ GeV) can be very difficult and inaccurate; it is delicate to disentangle the jet energy from the underlying event energy. Moreover the variables (6) lead to smoother theoretical distributions in the regions $x_{(LL)}^\pm \simeq 1$, which may be useful if one wants to compare theory with data for

these values of $x_{(LL)}^\pm$. These points have been discussed in more detail in ref. [10] to which we refer the interested reader.

Before using these variables, let us consider the behaviour of the photon-jet cross section with respect to the photon and jet rapidities. In order to enhance the direct-resolved contribution, we choose a large value of η_{jet} , $1 \leq \eta_{jet} \leq 2$, and we vary η_γ . The jets are defined in agreement with the cone algorithm used by the OPAL collaboration [13], with a cone radius $R = 1$ and a cut on the minimum value of E_T^{jet} that we fix equal to 3 GeV [18]. We also fix $p_T^\gamma = 5$ GeV. Our results are shown in Fig. 6 and they can be compared to those displayed in Fig. 5.

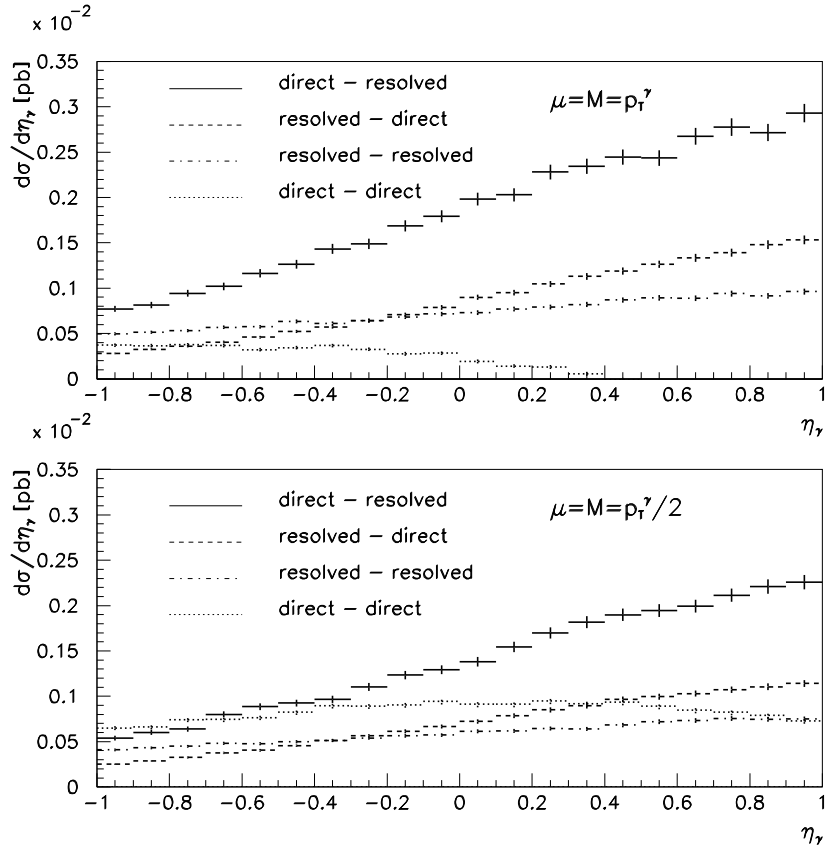


Figure 6: The cross sections $d\sigma^{\gamma+jet}/d\eta_\gamma$ at $p_{T\gamma} = 5$ GeV and $1 \leq \eta_{jet} \leq 2$ for two different scale choices.

We recall that, as always, the individual contributions to the total cross section have no physical meaning. Their relative importances are scale dependent. However, choosing e.g. the scales $\mu = M = p_{T\gamma}/2$ does not modify the fact that the direct-resolved contribution dominates in the range $\eta_\gamma \gtrsim -0.7$. Fig. 6 shows the enhanced direct-resolved contribution, corresponding to small values of $x_{(LL)}^-$ and large values of $x_{(LL)}^+$ in expressions (5) or (6), for the two scale choices $\mu = M = p_{T\gamma}$ and $\mu = M = p_{T\gamma}/2$. Hence, by working at large photon and jet rapidities, we can enhance the direct-resolved contribution and study its behaviour as a function of $x_{(LL)}^-$.

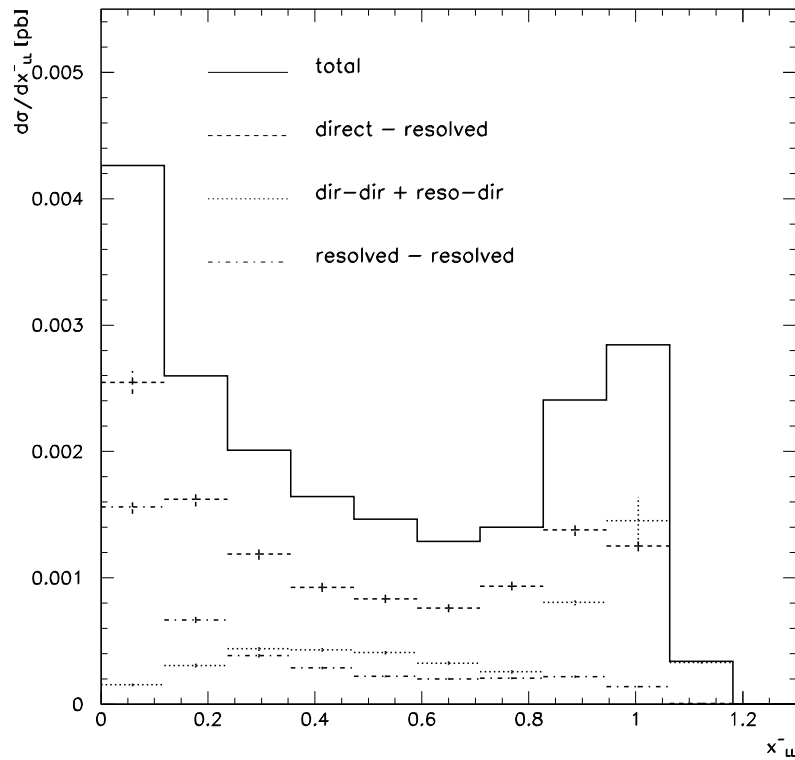


Figure 7: $d\sigma^{\gamma+jet}/dx_{LL}^-$ with $p_{T\gamma} = 5$ GeV, $1 \leq \eta_{jet} \leq 2$ and $0.5 \leq \eta_\gamma \leq 1$.

In Fig. 7 we display the distribution $d\sigma/dx_{LL}^-$ obtained with $p_{T\gamma} = 5$ GeV, $1 \leq$

$\eta_{jet} \leq 2$ and $0.5 \leq \eta_\gamma \leq 1$. The contributions from direct-direct and resolved-direct have been summed up in Fig. 7 since at $x^- \simeq 1$ there are large cancellations between these two contributions due to the finite remainders of the initial state collinear singularities, as has been explained in Section 2.1. This is illustrated in Fig. 8(a). Of course there are also cancellations between the direct-resolved and the direct-direct part, but those are of major importance in the x^+ spectrum for $x^+ \simeq 1$, affecting the x^- distribution only marginally.

Thus we can conclude from Fig. 7 that in the domain $x_{LL}^- \lesssim 0.8$ the cross section $d\sigma^{\gamma+jet}/dx_{LL}^-$ is quite sensitive to the parton distributions $F_{a/\gamma}(x_\gamma^- \sim x_{LL}^-, p_{T_\gamma})$ in the photon.

Until now we have used the variable x_{LL} to study the various contributions to the cross section $d\sigma/dx$. The use of x^\pm as defined in eq. (5) leads to a similar result, except around $x \simeq 1$ where the cross section $d\sigma/dx_{LL}$ has a smoother behaviour, as illustrated in Fig. 8 (b).

Fig. 9 shows that the contribution from the subprocess $\gamma + g \rightarrow q + \gamma + \bar{q}$ contributing to the direct-resolved part of $d\sigma/d\eta_\gamma$ is very small, and even negative for $\eta_\gamma > 0$, such that the full direct-resolved contribution is slightly *lower* than the one where g^γ has been set to zero. Thus the sensitivity to the gluon distribution in the photon as shown in Fig. 9(a) is basically due to the double resolved part in the present study.

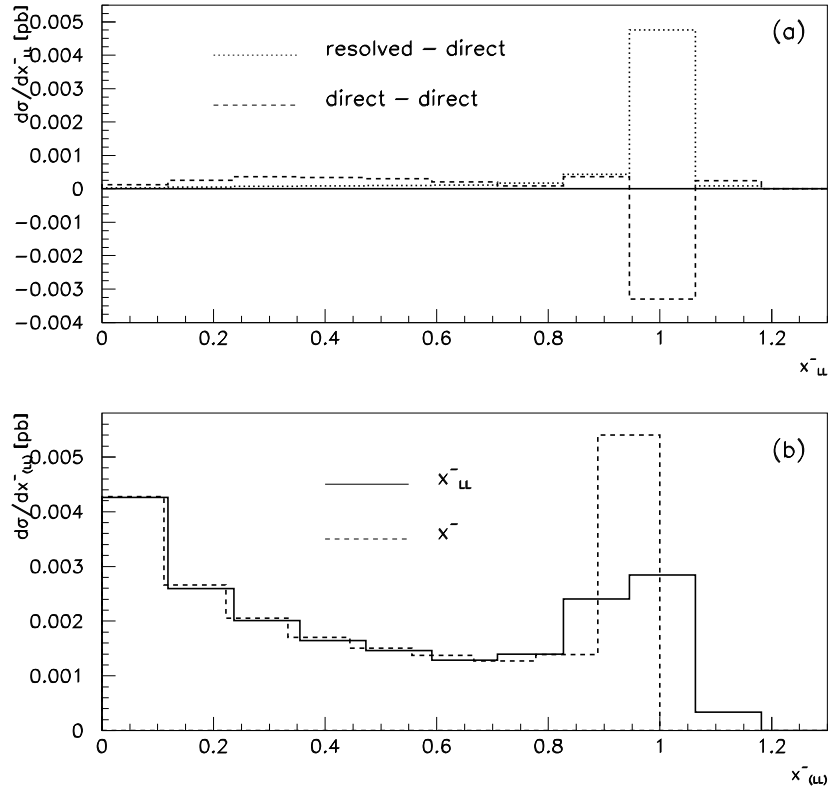


Figure 8: $d\sigma^{\gamma+jet}/dx_{(LL)}^-$ with $p_{T\gamma} = 5 \text{ GeV}$, $1 \leq \eta_{jet} \leq 2$, $0.5 \leq \eta_\gamma \leq 1$.
 (a) cancellations between resolved-direct and direct-direct subprocesses
 (b) comparison between $d\sigma^{\gamma+jet}/dx_{LL}^-$ and $d\sigma^{\gamma+jet}/dx_{\omega}^-$ (for the sum of all subprocesses). The distribution in x_{LL} shows a much smoother behaviour at $x \simeq 1$.

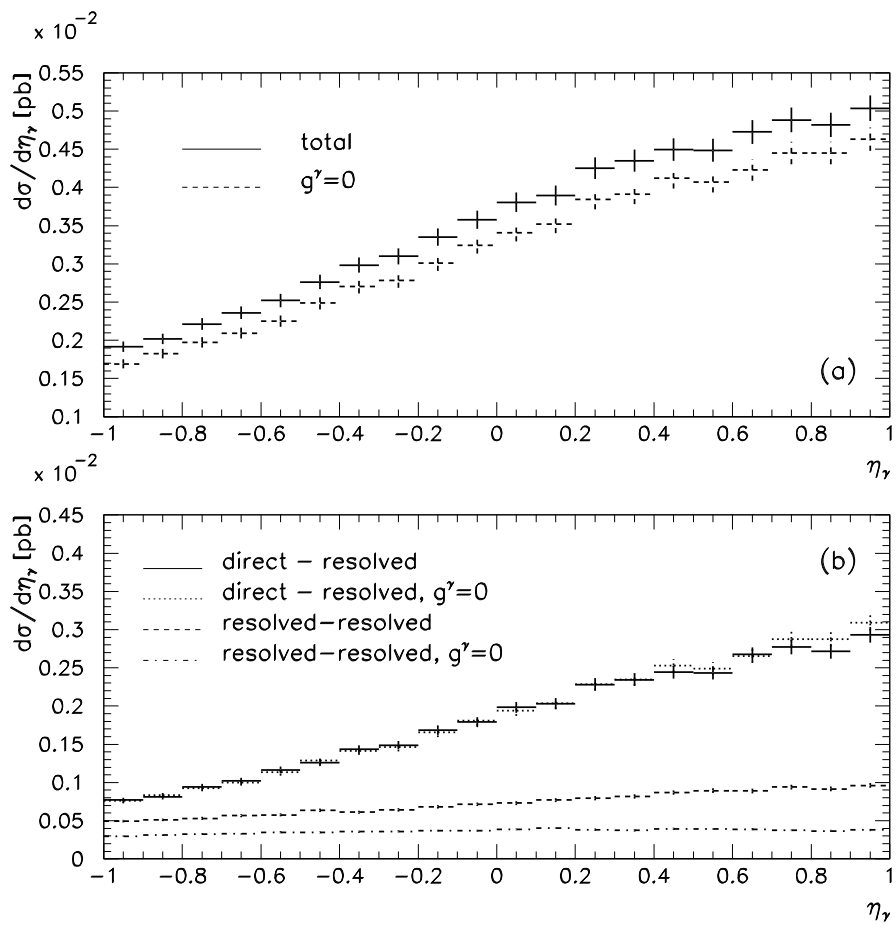


Figure 9: The contribution of the gluon in the resolved photon to the cross section $d\sigma^{\gamma+jet}/d\eta_\gamma$ at $p_{T\gamma} = 5$ GeV and $1 \leq \eta_{jet} \leq 2$.

4 Comparison with OPAL data

Before comparing theoretical predictions and data we have to assess the validity of the Weizsäcker-Williams (WW) approximation embedded in formula (1). This approximation is obviously correct as long as the photon virtuality is negligible with respect to the scale involved in the hard subprocess, namely $p_{T\gamma}$. But in OPAL $Q_{max}^2 \simeq 10 \text{ GeV}^2$ is of the order of the subprocess scale, $p_{T\gamma} \geq 3 \text{ GeV}$, and higher twist contributions proportional to $Q_{max}^2/p_{T\gamma}^2$ are not a priori negligible.

However we have to note that the Weizsäcker-Williams formula is dominated by the term $\sim \log(Q_{max}^2/m_e^2)$ which is very large (~ 27) because of the small mass of the electron; therefore the WW approximation should not be too bad, even if $Q_{max}^2/p_{T\gamma}^2 \simeq 1$.

Moreover the large virtuality of the incoming photon questions the use of parton distributions in real photons. To estimate the importance of the corrections due to the photon virtuality, let us consider the perturbative quark distribution in a real photon in the Born approximation

$$q_\gamma(x, M) = 3 \frac{\alpha}{2\pi} (x^2 + (1-x)^2) \int_{Q_0^2}^{M^2} \frac{dk^2}{k^2} \quad . \quad (7)$$

The lower limit Q_0^2 is the boundary below which a perturbative approach is no more valid. The value $Q_0^2 \simeq m_\rho^2 \simeq 0.5 \text{ GeV}^2$ leads to a photon structure function $F_2^\gamma(x, Q^2) = x \sum_q e_q^2 [q_\gamma(x, Q) + \bar{q}_\gamma(x, Q)]$ in agreement with DIS $\gamma^* \gamma$ experiments [17]. For a virtual photon, Q_0^2 must be replaced by $\max(Q^2, Q_0^2)$ and the convolution with the spectrum of the photon emitted by the electron takes the form

$$I = \int_{m_e^2}^{Q_{max}^2} \frac{dQ^2}{Q^2} \int_{\max(Q^2, Q_0^2)}^{M^2} \frac{dk^2}{k^2} \quad (8)$$

in which we drop all x -dependence. If $Q^2 > Q_0^2$, expression (8) can be written as the sum of the real photon expression and a correction

$$I = \int_{m_e^2}^{Q_{max}^2} \frac{dQ^2}{Q^2} \int_{Q_0^2}^{M^2} \frac{dk^2}{k^2} - \frac{1}{2} \text{Log}^2 \frac{Q_{max}^2}{Q_0^2} \quad . \quad (9)$$

For $Q_{max}^2 = 10 \text{ GeV}^2$, $Q_0^2 = 0.5 \text{ GeV}^2$ and $M^2 = p_{T\gamma}^2 = 25 \text{ GeV}^2$, the correction is of the order of 5 %. A similar estimation can be done for the non-perturbative part of the photon structure function with a correction of the order of 15 % which is also negative [19].

The conclusion of this study of the effects of the initial photon virtualities is that the WW approximation is valid in the OPAL kinematical range up to corrections of a few tens of percents.

Now we compare our results to OPAL preliminary data [13]. It has to be noted that in the experimental analysis the aim was to keep only events from single and double resolved processes. Therefore a component identified as stemming mainly from direct-direct events (denoted by "final state radiation" (FSR) in [13]) has been subtracted from the data. In a NLO calculation the final state radiation associated with the subprocess $\gamma\gamma \rightarrow \gamma q\bar{q}$ is a genuine contribution to the higher order corrections and thus cannot be removed from the total cross section. It can only be suppressed by an isolation criterion as discussed in Section 2.1. In the present study the isolated direct-direct contribution is small, such that it should not disturb the comparison with the preliminary OPAL data which have large experimental errors.

In Fig. 10 the cross section $d\sigma^{\gamma+X}/dp_{T\gamma}$ is shown. One observes that NLO theory is somewhat higher than the data, in particular at low $p_{T\gamma}$, but a correction term due to the rather large value of Q_{max}^2 would decrease the theory prediction (see eq. (9)), and including the FSR in the experimental analysis would increase the data. On the other hand, it is hard to estimate if higher twist effects (which should be non-negligible only at low $p_{T\gamma}$) would increase or decrease the theory prediction in the first $p_{T\gamma}$ -bin.

In short, taking into account a theoretical uncertainty of about 10 %, the agreement

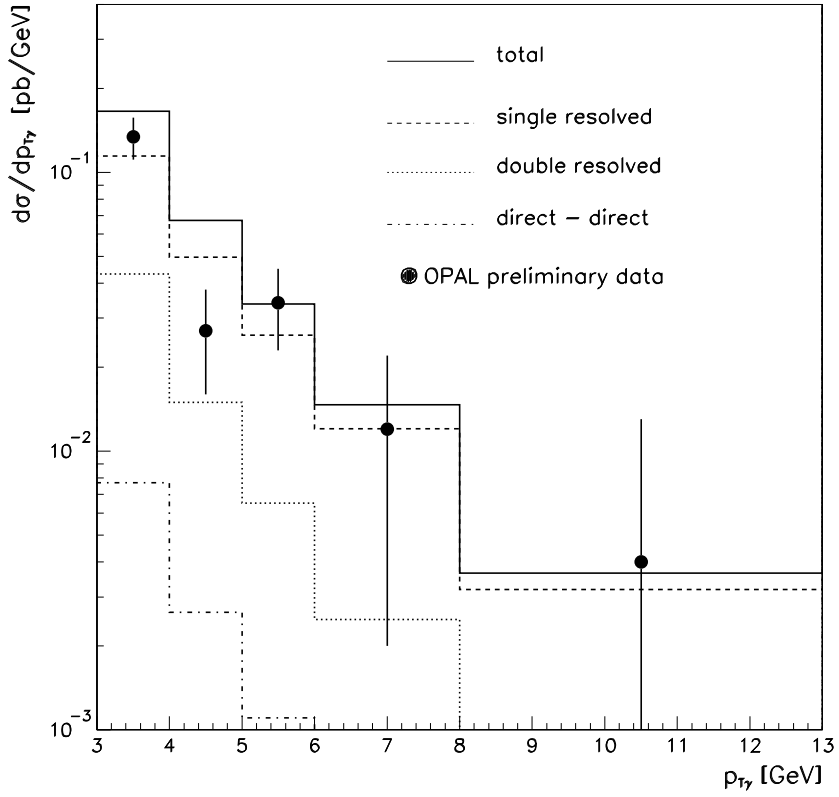


Figure 10: Comparison to preliminary OPAL data for $d\sigma^{\gamma+X}/dp_{T\gamma}$, integrated over photon rapidities in the range $-1 < \eta_\gamma < 1$, at the scales $\mu = M = p_{T\gamma}$.

with the data is completely satisfactory. The comparison to the rapidity distribution $d\sigma^{\gamma+X}/d|\eta_\gamma|$ is displayed in Fig. 11.

In [13] it is shown that PYTHIA reproduces the shapes of the distributions well, but has to be scaled up by a factor 1.85 to be consistent with the data. One reason for this difference in normalisation might be the use of different parton distribution functions for the photon (to obtain the PYTHIA result, SAS-1D [20] – which are LO fits – have been used).

We further note that the data are also compatible with our "leading order" result. This does not come as a surprise since the higher order corrections are small and

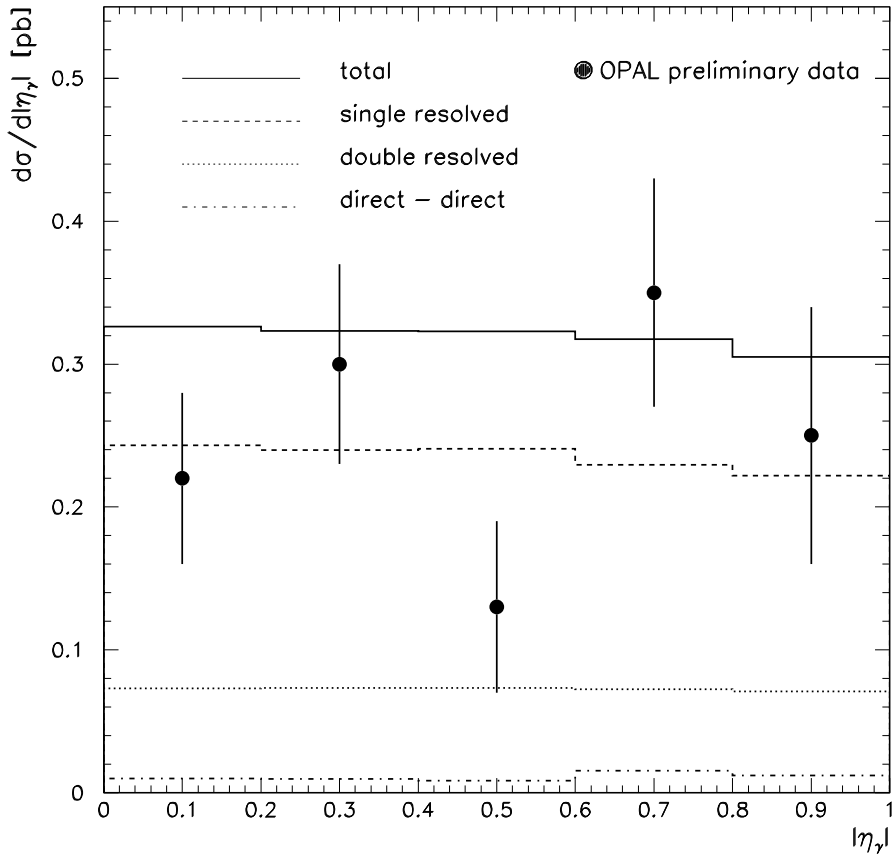


Figure 11: Comparison to preliminary OPAL data for $d\sigma^{\gamma+X}/d|\eta_\gamma|$, at the scales $\mu = M = p_{T_\gamma}$.

the preliminary data fluctuate a lot, but we recall that by "leading order" we only refer to the matrix elements and not to the parton distribution functions and α_s .

5 Conclusions

We have presented a complete NLO program for the calculation of the reactions $e^+e^- \rightarrow e^+e^-\gamma X$ and $e^+e^- \rightarrow e^+e^-\gamma + jet + X$, where the prompt photon is isolated using the criterion of S. Frixione [11]. The higher order corrections turned out to be of the order of 20% and the scale dependence is very weak: The total cross section varies by less than 5% if the scales are varied between $\mu = M = p_{T\gamma}/3$ and $3p_{T\gamma}$.

We discussed the possibility to constrain the parton distributions in the photon. For the photon-jet cross section, we have shown that one can enhance the direct-resolved component of the cross section by restricting the photon and jet rapidities to large values.

Further, we discussed the validity of the Weizsäcker-Williams approximation for a comparison to OPAL data with a rather large maximal photon virtuality of $Q_{\max}^2 = 10 \text{ GeV}^2$. The theoretical uncertainties introduced by using the parton distributions of real photons are also estimated in this context.

We compared the photon p_T and rapidity distribution for the $\gamma\gamma \rightarrow \gamma + X$ cross section to preliminary OPAL data [13]. In view of the large experimental errors, the agreement is good.

Acknowledgements

We would like to thank Stefan Söldner-Rembold from the OPAL collaboration for providing us the preliminary data and for helpful comments. This work was supported by the EU Fourth Training Programme "Training and Mobility of Researchers", network "Quantum Chromodynamics and the Deep Structure of Elementary Particles", contract FMRX-CT98-0194 (DG 12 - MIHT).

References

- [1] ZEUS collaboration, J. Breitweg et al., Eur. Phys. J **C11** (1999) 35;
H1 collaboration, C. Adloff et al., Eur. Phys. J **C1** (1998) 97.
- [2] S. Frixione and G. Ridolfi, Nucl. Phys. B **507** (1997) 315.
- [3] M. Klasen and G. Kramer, Z. Phys. C **76** (1997) 67;
M. Klasen, T. Kleinwort and G. Kramer, Eur. Phys. J. direct C **1** (1998) 1.
- [4] B. W. Harris and J. F. Owens, Phys. Rev. D **56** (1997) 4007.
- [5] P. Aurenche, L. Bourhis, M. Fontannaz and J. Ph. Guillet, Eur. Phys. J. C **17** (2000) 413.
- [6] L. E. Gordon and J. K. Storrow, Z. Phys. C **63** (1994) 581.
- [7] L. E. Gordon and W. Vogelsang, Phys. Rev. D **52** (1995) 58;
L. E. Gordon, Phys. Rev. D **57** (1998) 235.
- [8] M. Krawczyk, A. Zembrzuski, hep-ph/9810253 and hep-ph/0105166.
- [9] M. Fontannaz, J. Ph. Guillet and G. Heinrich, Eur. Phys. J. C **21** (2001) 303.
- [10] M. Fontannaz, J. Ph. Guillet and G. Heinrich, hep-ph/0107262, accepted for publication in Eur. Phys. J. C.
- [11] S. Frixione, Phys. Lett. **B429** (1998) 369.
- [12] S. Catani, M. Fontannaz, J. Ph. Guillet and E. Pilon, in preparation.
- [13] OPAL collaboration, OPAL Physics Note PN492.
- [14] M. Drees and R. M. Godbole, Phys. Lett. B **257** (1991) 425;
J. Phys. G **21** (1995) 1559.
- [15] L. E. Gordon and J. K. Storrow, Phys. Lett. B **385** (1996) 385.

- [16] T. Binoth, J. Ph. Guillet, E. Pilon, M. Werlen, Eur. Phys. J **C16** (2000) 311.
- [17] P. Aurenche, J. Ph. Guillet and M. Fontannaz, Z. Phys. **C64** (1994) 621.
- [18] G. Abbiendi *et al.* [OPAL Collaboration], Eur. Phys. J. C **10** (1999) 547.
- [19] P. Aurenche, J. Ph. Guillet, M. Fontannaz, Y. Shimizu, J. Fujimoto and K. Kato, Prog. Theor. Phys. **92** (1994) 175.
- [20] G. A. Schuler and T. Sjostrand, Z. Phys. C **68** (1995) 607.